Materials Chemistry and Physics 188 (2017) 95–99

Contents lists available at ScienceDirect

Materials Chemistry and Physics

journal homepage: www.elsevier.com/locate/matchemphys

Low cost oxide-based deposition of Cu_2FeSnS_4 thin films for photovoltaic absorbers

Guilin Chen [a, b, *, 1], Jianmin Li [c, 1], Shuiyuan Chen [a, b], Zhigao Huang [a, b], Miaoju Wu [a, b], Jifu Zhao [a, b], Weihuang Wang [a, b], Haiqin Lin [a, b], Changfei Zhu [c, **]

[a] Fujian Provincial Key Laboratory of Quantum Manipulation and New Energy Materials, College of Physics and Energy, Fujian Normal University, Fuzhou 350007, China

[b] Fujian Provincial Collaborative Innovation Center for Optoelectronic Semiconductors and Efficient Devices, Xiamen 361005, China

[c] CAS Key Laboratory of Materials for Energy Conversion, Department of Materials Science and Engineering, University of Science and Technology of China, Hefei 230026, China

HIGHLIGHTS

- A novel, low cost oxides nanoparticles-based process is introduced to deposit Cu_2FeSnS_4 thin films.
- The pure Cu_2FeSnS_4 films with large grains were obtained by sulfurizing oxides films.
- The CITS exhibits a band gap of 1.57 eV and obvious photo-electric response.

ARTICLE INFO

Article history:
Received 4 July 2016
Received in revised form
16 November 2016
Accepted 12 December 2016
Available online 13 December 2016

Keywords:
Chalcogenides
Thin films
Annealing
Semiconductors

ABSTRACT

In this study, a simple and novel oxide-nanoparticles-based process was applied to prepare Cu_2FeSnS_4 (CITS) thin films. Firstly, the low cost and naturally abundant oxides (e.g. CuO, Fe_2O_3 and SnO_2) were coated on the glass substrate. Secondly, CITS thin films were grown through the sulfurization of oxides precursors in a low toxic sulfur atmosphere. To investigate the phase transformation during sulfurization, the different annealing temperatures were used. It was found that the intermediate phase Cu_3SnS_4 and $Cu_2Sn_3S_7$ existed during the CITS growth. Finally, the phase-pure CITS films with large grains were obtained when the sulfurization temperature increased to 580 °C. Furthermore, an obvious photoelectric response of CITS thin film is displayed, which suggests its potential application as one kind of low cost solar absorber materials.

1. Introduction

Recently, the I_2–II–IV–VI_4 group semiconductors, such as $Cu_2Zn(Fe)Sn(S_xSe_{1-x})_4$, has attracted lots of attentions as a possible kind of absorber materials for thin films solar cells (TFSC), because of their interesting photoelectric properties and earth-abundant composition. For example, $Cu_2ZnSn(S,Se)_4$ (CZTSSe) thin films solar cell has been extensively studied, which has achieved an efficiency of 12.6% [1]. In addition, another alternative absorbing material Cu_2FeSnS_4 (CITS) has been attracted a lot of attentions as well. Because it has similar advantages with CZTSSe, such as high absorption coefficient (~10^4 cm^{-1}), proper band gap (~1.5 eV) and abundant elements [2]. However, the research on the application of CITS thin film solar cells remains rare. Only a few methods, such as sputtering [3], nanoparticles process [2,4], spray pyrolysis [5], and Aerosol-Assisted Chemical Vapor Deposition (AACVD) [6] have been created for the preparation of CITS thin films. Among them, nanoparticles-based process is one of the successful and low-cost approaches with high material utilization for the formation of thin films. This process is proven to be one of the successful non-vacuum approaches to $Cu(In,Ga)Se_2/Cu_2ZnSnS_4$ (CIGS/CZTS) formation, with variations employing particles composed of quaternary (CIGS/CZTS), oxides, metal, blended binary/ternary and binary

* Corresponding author. Fujian Provincial Key Laboratory of Quantum Manipulation and New Energy Materials, College of Physics and Energy, Fujian Normal University, Fuzhou 350007, China.
** Corresponding author.
E-mail addresses: glchen@fjnu.edu.cn (G. Chen), cfzhu@ustc.edu.cn (C. Zhu).
[1] These authors contributed equally to this work.

http://dx.doi.org/10.1016/j.matchemphys.2016.12.024
0254-0584/

sulfide nanoparticles as precursor [7]. However, to the best of our knowledge, only CITS quaternary nanoparticles were applied as precursor for the fabrication of CITS thin films so far, although many methods were applied to synthesize CITS quaternary nanoparticles, such as hot injection [2], and solution based synthesis [8], thermal decomposition [9], solvothermal method [10].

On account of the oxide nanoparticles process could have a great degree control of component of the final thin films during the reaction pathway [7,11,12]. Meanwhile, the using of oxides as precursors can effectively reduce the preparation cost, which can be synthesized by a simple solid state reaction. It is available to avoid the aggregation of nanoparticles when there is no solvent during the whole reaction [13]. Therefore, the oxide nanoparticles process is regarded as an extremely promising method for the deposition of CIGS and CZTS thin films. However, this method hasn't been used for preparing CITS thin films until now. In this paper, we adopted a neoteric oxide nanoparticles-based method for the facile preparation of high quality CITS thin films. Because the oxides used in this work are quite stable and abundant in earth (e.g. CuO, Fe_2O_3 and SnO_2), such a method can efficiently reduce the cost of preparation. In addition, the effects of sulfurization temperatures on the structures and morphology of CITS were also carefully investigated.

2. Experimental

Firstly, the powder of oxides was prepared by a solvent-free method, which was similar to our previous report [7]. In this experiment, 0.02 mol $Cu(NO_3)_2{\cdot}3H_2O$, 0.01 mol $Fe(NO_3)_2{\cdot}9H_2O$, 0.01 mol SnC_2O_4 (the Cu:Fe:Sn ratio corresponded to 2:1:1) and excess ammonium bicarbonate (0.1 mol) were mixed thoroughly and then ground for 10 min. Subsequently, the mixture was heated at 380 °C for an hour to obtain oxide powder which was deposited on the glass substrates in thin layers through doctor blade process later. Finally, the sulfurization process of the oxide layers was carried out in low toxic sulfur vapor at various temperatures (430, 480, 530 and 580 °C) for 30 min.

The crystal structure of the powder and films were identified by X-ray diffraction (XRD, Rigaku D/Max-rA). The morphology of film was observed by a field emission scanning electron microscope (FESEM, JEOL-JSM-6700F, equipped with energy dispersive X-ray spectroscopy (EDX)). The Raman tests were performed using a Raman spectrometer system (Horiba-Jobin Yvon, LabRam-HR) with a laser source of 532 nm. The X-ray photoelectron spectroscopy (XPS) spectra were carried out on thermo ESCALAB 250 spectrometer. The optical absorption spectrum was recorded on a UV–vis-365-type spectrophotometer. I-V curves were measured by Keithley Instruments (4200S) under dark and simulated AM 1.5 G spectrum at 100 mW/cm^2 (1 sun) illumination, respectively. The 4-point probe method was also used to measure the electrical properties of the thin films. The film thicknesses were measured using surface step profiler (Dektak-XT).

3. Results and discussions

Fig. 1(a) shows the XRD patterns of the as synthesized oxide powders, which were obtained from the solid state reaction. All the X-ray peaks have been indexed, which confirmed the formation of CuO, Fe_2O_3 and SnO_2. According to the XRD patterns, it can be clearly found that the preferred orientation of the CuO, Fe_2O_3 and SnO_2 phase are (0 0 2), (1 1 6) and (1 1 0) respectively. Sequentially, the oxide nanoparticles were used to mix with ethanol to form oxides nanoparticles ink which was absent of any other organic additives. During the coating process, the ethanol dispersing agent will evaporate quickly, leaving carbon-free oxides precursor films. The planar SEM micrographs of the precursor films (Fig. 1(b)) revealed a smooth, uniform and crack-free film over a large area, which would be the key to grow homogeneous and dense CITS films. Though some pinholes are observed on the surface of the precursor thin films, it can be eliminated by the densification during sulfurization. It is due to the fact that partial substitution of the larger size S atom (1.84 Å) for the smaller size O atom (0.65 Å) can make volume expansion. In the beginning, all the oxides react with the sulfur to create sulfides during the process of sulfurization. In order to determine the difficulty level of converting metallic oxides to metallic sulfide in the annealing process, the Ellingham diagram of Metal(M)–O–S was calculated by using the Gibbs free energy of formation (Fig. 1(c)). As the sulfurization is carried out in sulfur atmosphere, the reaction can be described with the following equation:

$$2MO_x(s) + 1.5xS_2(g) \rightarrow 2MS_x(s) + xSO_2(g) \quad (M: Cu, Zn, Sn; x = 1 \ or \ 2) \tag{1}$$

All reactions are able to occur spontaneously, which are attributed to the minus Gibbs free energies (ΔG). It is notable that the above reactions can be activated within a wide temperature range [14]. As shown in Fig. 1(c), the lower the lines are, the more active the oxides will be. Thus, the stability of these oxides should be: $SnO_2 > Fe_2O_3 > CuO$. As the sulfurization temperature increased, all the oxides were completely converted into binary sulfides. Finally, the CITS thin films were generated from the binary sulfides at high temperature.

Fig. 2(a) shows the XRD patterns of CITS thin films which were sulfurized at 430, 480, 530 and 580 °C respectively. The process of forming pure-phase CITS with the increase of the sulfurization temperature can be observed from these XRD patterns. In this part, all diffraction peaks can be indexed to the stannite structured CITS

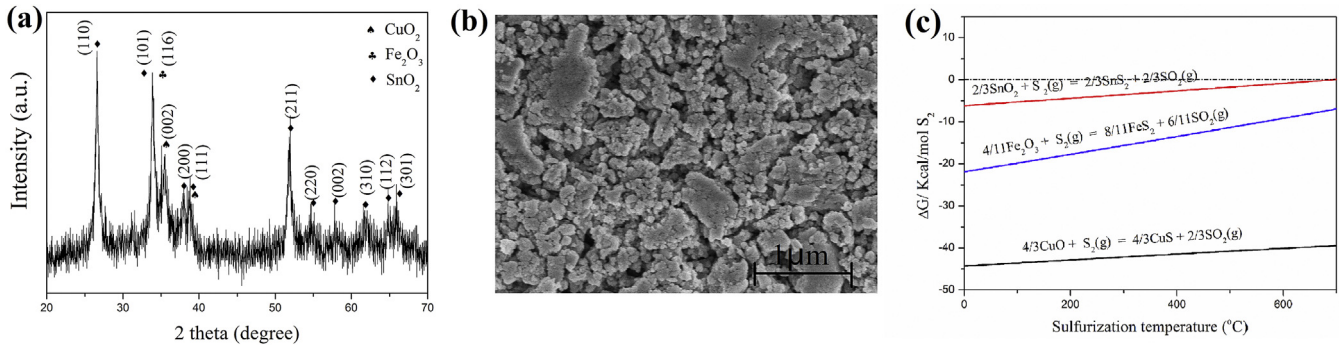

Fig. 1. (a) The XRD patterns of oxides powder, (b) SEM of oxides precursor films, and (c) Ellingham diagram for the Metal–O–S system.

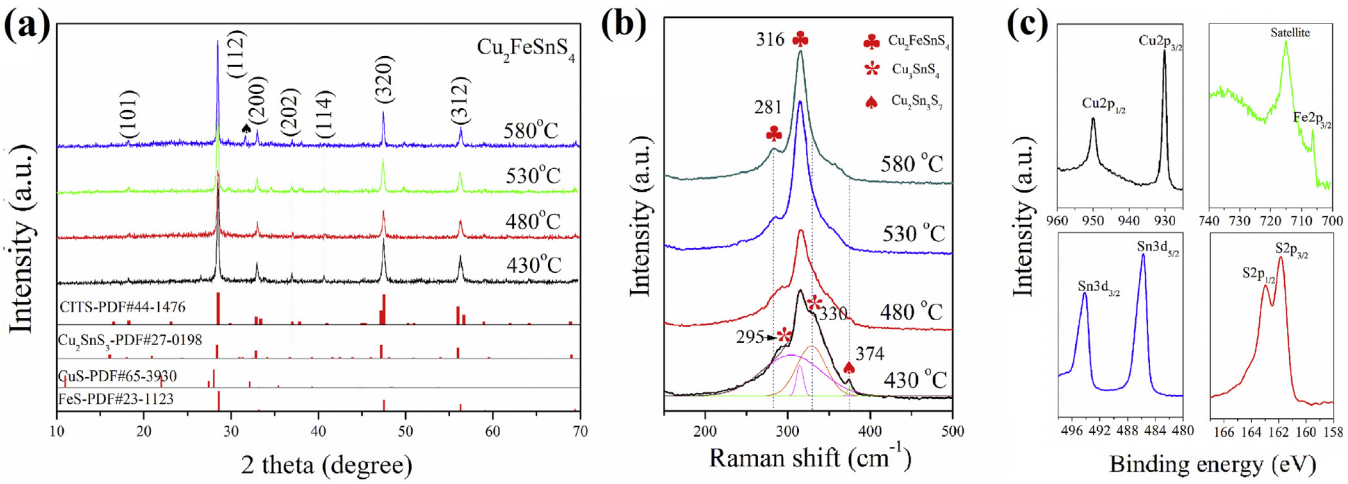

Fig. 2. (a) The XRD patterns, (b) Raman of films sulfurized at different temperatures, and (c) XPS analysis on CITS films annealed at 580 °C.

with preferential orientation in the (1 1 2) plane (JCPDS, no. 44-1476). And the main diffraction peaks appeared at $2\theta = 28.4°$, 47.4° and 56.4° are corresponded well with (1 1 2), (2 2 0) and (3 1 2) planes of stannite structured CITS. Besides, the calculated lattice parameters are a = 5.41 Å and c = 10.81 Å, which are in very good agreement with the published data from Cao et al. [15]. However, XRD cannot allow us to make a clear distinction between CITS and other possible tiny secondary phases such as Cu_2SnS_3. In the contrary, Raman scattering is a useful technique to identify the secondary phases. Fig. 2(b) shows the Raman spectra of the CITS thin films annealed at different temperatures. For all the CITS samples, Raman peaks at 281 and 316 cm^{-1} are observed, which can be attributed to CITS [16]. As the annealing temperature is up to 430 °C, the Raman peaks corresponding to Cu_3SnS_4 and $Cu_2Sn_3S_7$ were observed at 330 and 374 cm^{-1} [17,18]. When the temperature continues to increase, all the annealed films showed pure-phase CITS without any Cu_xSnS_y impurity. So the minimum sulfurization temperature, as well as minimum energy for phase formation, is about 480 °C. In addition, XPS was applied to determine the valence states of CITS thin films sulfurized at 580 °C. In Fig. 2(c), the Cu 2p core splits into $2p_{3/2}$ (930.3 eV) and $2p_{1/2}$ (950.1 eV) peaks, which are characteristic of Cu^+. Two peaks of Fe 2p and Sn 3d located at 706.5/715.0 eV and 485.8/494.2 eV, which suggests the existence of Fe^{2+} and Sn^{4+} respectively [8,19]. The peaks observed at 161.8 and 162.9 eV are corresponded for S in sulfide phases. Combining with the analyses of XPS, Raman and XRD, it can conclude that the pure CITS phase can be obtained by sulfurizing the oxide precursors at 580 °C. The general chemical reactions occurred during the sulfurization process were described as follows:

$$4CuO + Fe_2O_3 + 2SnO_2 + 6.75S_2(g) \rightarrow 2Cu_2FeSnS_4 + 5.5SO_2(g) \quad (2)$$

During the growth CZTS phase, another reaction path has been proven, in which the intermediate phase Cu_3SnS_4 and Cu_2SnS_3

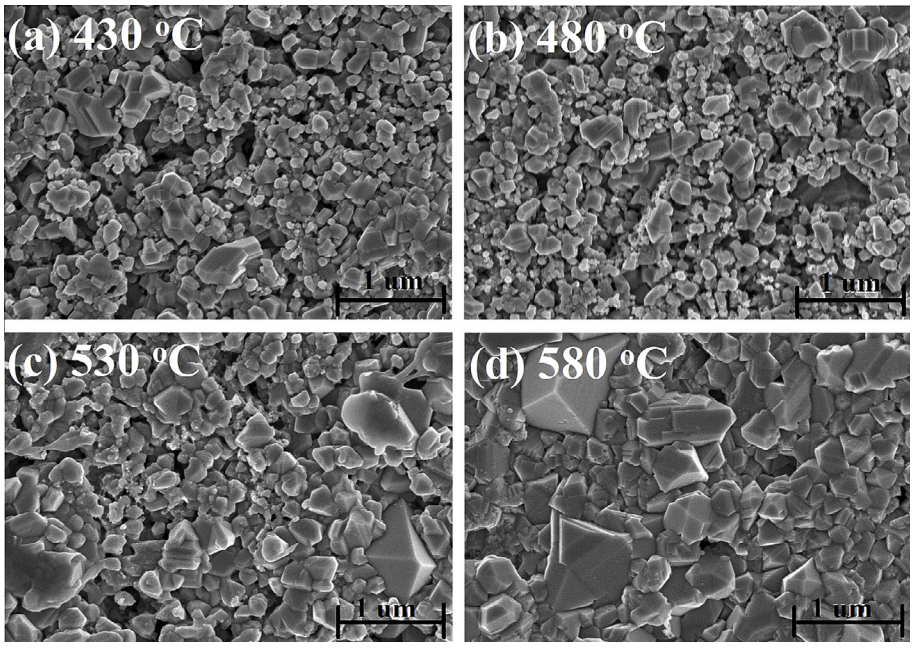

Fig. 3. SEM of CITS thin films annealed at different temperatures.

Table 1
The composition of the CITS films annealed at 580 °C determined by EDX[a].

Element	Cu	Fe	Sn	S
Atom%	23.99	11.77	10.24	54.00

[a] These ratios calculated from semi-quantitative EDX data may contain 10% error.

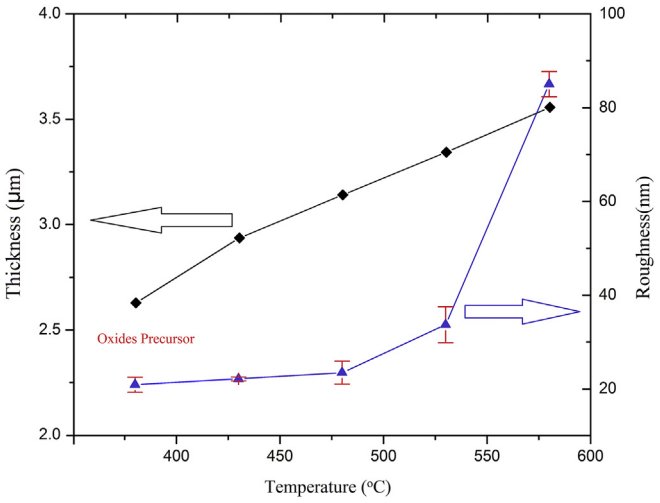

Fig. 4. The thickness and roughness of CITS thin films annealed at different temperatures.

were firstly created and then reacted with ZnS to form CZTS. Such a reaction path with intermediate compound was also observed during the CITS growth, except the different intermediate phase $Cu_xSn_yS_z$ was generated. The above temperature dependent Raman measurements indicated that our CITS formation underwent a favorable pathway through the intermediate phase Cu_3SnS_4 and $Cu_2Sn_3S_7$. It suggested that there were mainly four possible reactions once the binary sulfides were formed:

$$3CuS + SnS_2 \rightarrow Cu_3SnS_4 + 0.5S_2(g) \quad (3)$$

$$2Cu_3SnS_4 + 3FeS_2 + SnS_2 \rightarrow 3Cu_2FeSnS_4 + 2S_2(g) \quad (4)$$

$$2CuS + 3SnS_2 \rightarrow Cu_2Sn_3S_7 + 0.5S_2(g) \quad (5)$$

$$Cu_2Sn_3S_7 + 3FeS_2 + 4CuS \rightarrow 3Cu_2FeSnS_4 + 2.5S_2(g) \quad (6)$$

The SEM micrographs of the CITS films annealed at various temperatures are shown in Fig. 3. As we can observe, the increasement of the sulfurization temperature markedly improves the crystallinity and the grain size of films, which is due to the high thermal energy supplied the driving force to coalesce the grains. The CITS films sulfurized at 580 °C show a densely packed morphology with large grains. The chemical composition ratio of Cu:Fe:Sn:S is about 23.99:11.77:10.24:54.00, which is indicated by the EDX of CITS thin films annealed at 580 °C, as seen in Table 1. Taking the measuring error (10%) of EDX into consideration [20], this composition is almost corresponding to that of the starting material. The slight deviation of the chemical compositions was mainly caused by the reactivity of different metal precursors, which can be deduced from the above thermo mechanical analysis [21]. Such a phenomenon has also been described by the previous works, which seem to be acceptable [22,23]. So there is no significant loss of elements during the synthesis of the particles, coating steps and annealing. In other words, such process shows good compositional control.

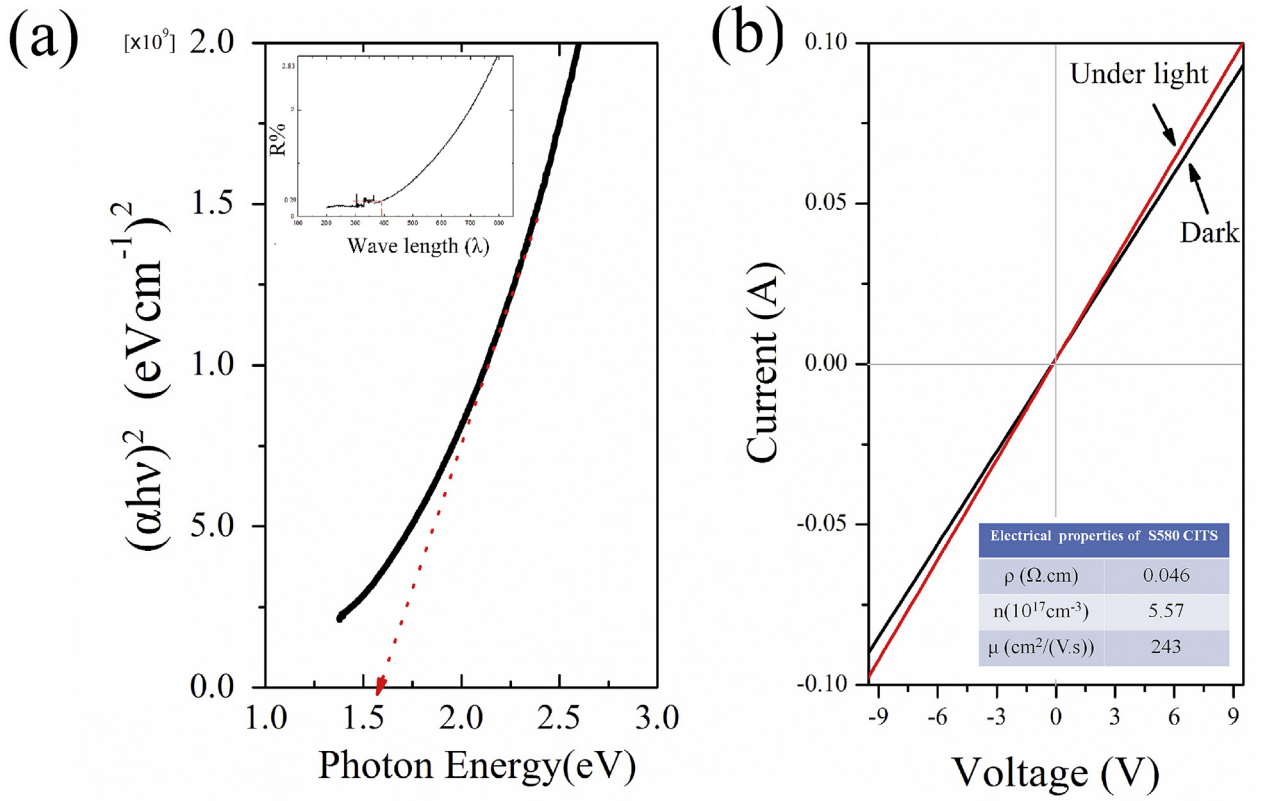

Fig. 5. (a) Plot of $(\alpha h\nu)^2$ vs hν for the estimation of the band gap energy of S580-CITS thin film, inset: the optical reflectance spectra; (b) The I–V curve of the S580-CITS thin film tested in the darkness and under illumination, inset: Electrical properties of S580 CITS.

In order to study the effects of annealing temperature on the CITS thin films, the surface step profiler measurement was also carried out. The results were compared with oxide precursor thin films. Fig. 4 shows the thickness and roughness of the CITS thin films annealed at different temperature. It can be seen that the thickness was increased as the annealing temperature increased. This is caused by the volume expansion during sulfurization (small oxygen atom was replaced by big sulfur atom), which was also observed in the oxide-derived CIGS and CZTS thin films. Meanwhile, the roughness of CITS was tested in this work. The oxides precursor films were essentially smooth. As the precursor was suffered from sulfurization annealing, the roughness increases with the increasing sulfurization temperature. The roughness gradually increases as sulfurization temperature up to 530 °C. However, it rapidly increases to 87 nm when the sulfurization temperature reaches 580 °C. This is due to the grain growth of CITS thin films during the sulfurization. The higher annealing temperature was used, the higher driving force for grain growth was obtained. So the CITS with very large grain size can be prepared under high temperature sulfurization. The large grain on the surface will result a large roughness value. This agrees well with the SEM observation. It is well known that the efficiency of polycrystalline solar cells increases with improvement in quality of the absorber layer. So the dense oxides-derived CITS thin films with near stoichiometric composition can be applied in CITS TFSC.

Fig. 5(a) shows the optical reflectance spectrum and band gap estimation of S580-CITS thin film. The inset reveals that CITS absorber material has excellent optical property for its high absorptivity towards visible light. The average absorptivity of CITS absorber material towards visible light is above 98%, that means CITS absorber material can absorb almost all of visible light. Combining with thickness of S580-CITS (3.5 μm), the absorption coefficients of S580-CITS thin films are calculated to be above $2^{*}10^{4}$ cm^{-1} in the visible range. This high absorption coefficient is suitable for the absorber layer in a thin film solar cell. In addition, the energy band gap of the CITS thin film has been obtained by extending the liner portion of the relation curve between $(\alpha h\nu)^2$ and $h\nu$ (α = absorbance, h = Planck's constant and ν = frequency). As shown in Fig. 5(a), the energy band gap of the CITS thin film is about 1.57 eV, which is closed to the optimal band gap (1.5 eV) for absorption. The above band gap value match well with the value reported for CITS thin film [24]. To investigate the photoelectric properties, the current–voltage (I–V) measurements for the S580-CITS thin films were performed. Fig. 5(b) shows the I–V curves of the films tested in the darkness and under an illumination intensity of 100 $mW{\cdot}cm^{-2}$ from a standard AM1.5G light source, which was measured in a 10 V bias range. It was found that an increase of about 10% in photocurrent at 10 V under light irradiation relative to the dark state. In the present case, the energy from light irradiation excites electrons in the CITS thin films from valance band to conduction band and then increases the holes in the film [25]. As a result, the current is increased markedly. The electrical properties of S580 CITS thin films were studied by Hall effect measurement employing a Van der Pauw method at room temperature. The S580 CITS thin films exhibited p-type conductivity as determined by Hall coefficient. The resistivity (ρ), carrier concentration (n) and mobility (μ) of the S580 CITS thin films are 0.046 Ω·cm, $5.57^{*}10^{17}cm^{-3}$ and 243 $cm^2/(V{\cdot}s)$ respectively, as shown in the insect of Fig. 5(b). Khadka et al. have revealed that the wide range of electrical parameters in chalcogenide compound depended on the fabrication technique and quality of samples [26]. The electrical parameters of S580 CITS thin films in this work are close to the results summarized by Khadka [26]. Therefore, the CITS films prepared by sulfurizing oxide precursors are suitable for applications in TFSC.

4. Conclusion

In conclusion, we have successfully demonstrated that the CITS thin films can be synthesized through the oxide-nanoparticles-based process which is a feasible and low cost non-vacuum approach. After the deposition and sulfurization of the oxide precursors that is the mixture of CuO, Fe_2O_3 and SnO_2, the dense CITS thin films with large grains were obtained. Moreover, the CITS thin films annealed at 580 °C exhibit a band gap of 1.57 eV and obvious photo-electric response. The electrical properties revealed p-type conductivity. The resistivity, carrier concentration and mobility are about 0.046 Ω·cm, $5.57^{*}10^{17}cm^{-3}$ and 243 $cm^2/(V{\cdot}s)$ for of the S580 CITS thin films, respectively. As a prospect of this study, it revealed a promising oxide-based way for the preparation of CITS thin films and promoting the pace of their application in CITS thin film solar cells.

Acknowledgment

This work was supported by National Natural Science Foundation of China (Grant No. 51502037), Natural Science Foundation of Fujian Province, China (Grant No. 2015J05096).

References

[1] W. Wang, M.T. Winkler, O. Gunawan, T. Gokmen, T.K. Todorov, Y. Zhu, D.B. Mitzi, Adv. Energy Mater. 4 (2014) 1301465.
[2] C. Yan, C. Huang, J. Yang, F. Liu, J. Liu, Y. Lai, J. Li, Y. Liu, Chem. Commun. 48 (2012) 2603–2605.
[3] X. Meng, H. Deng, J. He, L. Sun, P. Yang, J. Chu, Mater. Lett. 151 (2015) 61–63.
[4] J. Zhou, Z. Ye, Y. Wang, Q. Yi, J. Wen, Mater. Lett. 140 (2015) 119–122.
[5] D.B. Khadk, J. Kim, J. Alloy Compd. 638 (2015) 103–108.
[6] P. Kevin, M.A. Malik, P. O'Brien, New J. Chem. 39 (2015) 7046–7053.
[7] G. Chen, C. Yuan, J. Liu, Z. Huang, S. Chen, W. Liu, G. Jiang, C. Zhu, J. Power Sources 276 (2015) 145–152.
[8] L. Lia, X. Liu, J. Huang, M. Cao, S. Chen, Y. Shen, L. Wang, Mater. Chem. Phys. 133 (2012) 688–691.
[9] K. Mokurala, P. Bhargava, S. Mallick, Mater. Chem. Phys. 147 (2014) 371–374.
[10] Y. Cui, R. Deng, G. Wang, D. Pan, J. Mater. Chem. 22 (2012) 23136–23140.
[11] V.K. Kapur, A. Bansal, P. Le, O.I. Asensio, Thin Solid Films 431–432 (2003) 53–57.
[12] D. Tang, Q. Wang, F. Liu, L. Zhao, Z. Han, K. Sun, Y. Lai, J. Li, Y. Liu, Surf. Coat. Technol. 232 (2013) 53–59.
[13] G. Chen, B. Pan, L. Jin, G. Jiang, W. Liu, C. Zhu, J. Alloy Compd. 610 (2014) 20–26.
[14] G. Smestad, A. Ennaoui, S. Fiechter, H. Tributsch, W. Hofmann, M. Birkholz, W. Kautek, Solar Energy Mater. 20 (1990) 149–165.
[15] M. Cao, C. Li, B. Zhang, J. Huang, L. Wang, Y. Shen, J. Alloy Compd. 622 (2015) 695–702.
[16] C. Rincon, M. Quintero, E. Moreno, C. Power, E. Quintero, J.A. Henao, M.A. Macías, G.E. Delgado, R. Tovar, M. Morocoima, Solid State Commun. 151 (2011) 947–951.
[17] Z. Su, K. Sun, Z. Han, F. Liu, Y. Lai, J. Li, Y. Liu, J. Mater. Chem. 22 (2012) 16346–16352.
[18] D.M. Berg, R. Djemour, L. Gütay, S. Siebentritt, P.J. Dale, X. Fontane, V. Izquierdo-Roca, A. Perez-Rodriguez, Appl. Phys. Lett. 100 (2012) 192103.
[19] X. Liang, X. Wei, D. Pan, J. Nanomater. 2012 (2012) 708648.
[20] T. Todorov, M. Kita, J. Carda, P. Escribano, Thin Solid Films 517 (2009) 2541–2544.
[21] B. Zhang, M. Cao, L. Li, Y. Sun, Y. Shen, L. Wang, Mater. Lett. 93 (2013) 111–114.
[22] Q.J. Guo, G.M. Ford, W.C. Yang, B.C. Walker, E.A. Stach, H.W. Hillhouse, R. Agrawal, J. Am. Chem. Soc. 132 (2010) 17384–17390.
[23] D.B. Khadka, J. Kim, J. Phys. Chem. C 118 (2014) 14227–14237.
[24] B. Zhang, M. Cao, L. Li, Y. Sun, Y. Shen, L. Wang, Mater. Lett. 93 (2013) 111–114.
[25] L. Shi, Y. Li, RSC Adv. 4 (2014) 43720–43724.
[26] D.B. Khadka, J. Kim, J. Alloy Compd. 638 (2015) 103–108.